ADVANCED MATERIALS

Inc.) under vacuum for 30 min to selectively degrade the PMMA and crosslink PS, leaving behind the porous PS template.

Received: January 24, 2005
Final version: July 24, 2005
Published online: September 1, 2005

[1] I. W. Hamley, *The Physics of Block Copolymers*; Oxford University Press: New York, **1998**.
[2] G. H. Fredrickson, F. S. Bates, *Annu. Rev. Mater. Sci.* **1996**, *26*, 501.
[3] M. Lazzari, M. A. López-Quintela, *Adv. Mater.* **2003**, *15*, 1583.
[4] I. W. Hamley, *Angew. Chem. Int. Ed.* **2003**, *42*, 1692.
[5] R. E. Segalman, *Mater. Sci. Eng. Rev.* **2005**, *48*, 191.
[6] T. Thurn-Albrecht, J. Schotter, A. Kästle, N. Emley, T. Shibauchi, L. Krusin-Elbaum, K. Guarini, C. T. Black, M. T. Tuominen, T. P. Russell, *Science* **2000**, *290*, 2126.
[7] M. Park, C. K. Harrison, M. Chaikin, R. A. Register, D. H. Adamson, *Science* **1997**, *276*, 1407.
[8] A. M. Urbas, M. Maldovan, P. DeRege, E. L. Thomas, *Adv. Mater.* **2002**, *14*, 1850.
[9] H. Ma, A. K.-Y. Jen, L. R. Dalton, *Adv. Mater.* **2002**, *14*, 1339.
[10] J. T. Chen, E. L. Thomas, C. G. Zimba, J. F. Rabolt, *Macromolecules* **1995**, *28*, 5811.
[11] W. Knoll, *Annu. Rev. Phys. Chem.* **1998**, *49*, 569.
[12] W. Knoll, *MRS Bull.* **1991**, *16*, 29.
[13] J. D. Swalen, *J. Phys. Chem*. **1979**, *83*, 1438.
[14] E. Kretschmann, *Opt. Commun.* **1972**, *6*, 185.
[15] W. Knoll, in the *Handbook of Optical Properties Vol. II, Optical Properties of Small Particles, Interfaces and Surfaces*, (Eds.: R. E. Hummel, P. Wissmann) , CRC Press, Boca Raton, FL **1997**.
[16] U. Jeong, D. Y. Ryu, D. H. Kho, J. K. Kim, J. T. Goldbach, D. H. Kim, T. P. Russell, *Adv. Mater.* **2004**, *16*, 533.
[17] W. R. Thompson, M. Cai, M. Ho, J. E. Pemberton, *Langmuir* **1997**, *13*, 2291.
[18] J. W. Robertson, M. Cai, J. E. Pemberton, *Adv. Mater.* **2001**, *13*, 662.
[19] P. Mansky, T. P. Russell, C. J. Hawker, M. Pitsikalis, J. Mayes, *Macromolecules* **1997**, *30*, 6810.
[20] P. Mansky, Y. Liu, E. Huang, T. P. Russell, C. J. Hawker, *Science* **1997**, *275*, 1458.
[21] M. Maldovan, M. R. Bockstaller, E. L. Thomas, W. C. Carter, *Appl. Phys. B* **2003**, *76*, 877.
[22] C. G. Granqvist, O. Hunderi, *Phys. Rev. B* **1978**, *18*, 2897.
[23] A decrease of ε_D from 2.220 to 2.048 was calculated from comparison between the dielectric constant of the initial film ($\varepsilon_x = \varepsilon_y = 2.402$, $\varepsilon_z = 2.429$) and that of the porous template ($\varepsilon_x = \varepsilon_y = 2.377$, $\varepsilon_z = 2.385$). Then, the best fractional combination of air and PMMA was deduced to fit the effective constant of 2.048, using Equation 2.
[24] The film was subjected to the exposure conditions used to etch away PMMA domains in a thin PS-*b*-PMMA film of thickness ~L_0 (D. H. Kim, Z. Lin, H.-C. Kim, U. Jeong, T. P. Russell, *Adv. Mater.* **2003**, *15*, 811), which is about ten times thinner than the thickness used in this study.
[25] D. E. Aspnes, *Thin Solid Films* **1982**, *89*, 249.
[26] Note that the values of ε_{PBS} and ε_{EtOH} are 1.774 and 1.845, respectively.
[27] K. H. A. Lau, L.-S. Tan, K. Tamada, M. S. Sander, W. Knoll, *J. Phys. Chem. B.* **2004**, *108*, 10812.
[28] J. L. Wang, T. Grimaud, K. Matyjaszewski, *Macromolecules* **1997**, *30*, 6507.

Self-Organization of FePt Nanoparticles on Photochemically Modified Diblock Copolymer Templates**

By *Seth B. Darling*, *Nataliya A. Yufa*, *Amadou L. Cisse*, *Samuel D. Bader*, and *Steven J. Sibener**

Phase-segregated block copolymers have received significant attention in the last decade as enabling materials for future technologies.[1–6] Their value to nanotechnology derives from the expedient tunability of the size, shape, and periodicity of the self-assembled domains by means of manipulating molecular characteristics. Recently, the potential opportunities for block copolymer applications have been bolstered by new methods, which give fine control over long-range ordering of the microdomain structures.[4,5,7,9] Thin polymer films, by themselves, have limited device applications, but myriad functions can be addressed with hybrid hard/soft matter systems in which the organic layer is used as a scaffold for nanoscale organization of inorganic materials. Of specific interest is the interaction of surfactant-mediated colloidal nanoparticles and diblock copolymer films because the nanocrystal capping molecules can be tailored to exhibit preference for one of the polymer blocks.[10–13] This hierarchical approach to create ordered nanostructures removes the linear correlation of size and patterning time associated with traditional lithographic techniques by self-assembling the entire surface in parallel. Also, the spatial limits of lithography can be transcended and the approach can potentially be adapted to industrial-scale processing. An alternative approach to the colloidal nanocrystal methodology is to use spherical- or cy-

[*] Prof. S. J. Sibener, A. L. Cisse
James Franck Institute and Department of Chemistry
The University of Chicago
Chicago, IL 60637 (USA)
E-mail: s-sibener@uchicago.edu
Dr. S. B. Darling, Dr. S. D. Bader
Materials Science Division and Center for Nanoscale Materials
Argonne National Laboratory
Argonne, IL 60439 (USA)
N. A. Yufa
James Franck Institute and Department of Physics
The University of Chicago
Chicago, IL 60637 (USA)

[**] The authors thank Ward Lopes for useful discussions and A. C. Samia, J. Schleuter, and X. M. Lin for providing the FePt nanoparticles used in this study. The work was supported by the University of Chicago–Argonne National Laboratory Consortium for Nanoscience Research, the NSF-Materials Research Science and Engineering Center at The University of Chicago (NSF-DMR-0213745), and the AFOSR sponsored MURI Center for Materials Chemistry in the Space Environment. Work at Argonne is supported by the U.S. Department of Energy, Basic Energy Sciences-Materials Sciences, under Contract #W-31-109-ENG-38.

  DOI: 10.1002/adma.200500960

lindrical-phase diblock copolymers as etch masks to produce self-assembled arrays of nanoscale dots, pillars, or lines composed of various materials.[3,14–16] The advantage of our approach is that the length-scale of the final functional material is an order of magnitude smaller than the original polymer domains.

We have selected FePt nanoparticles because they are central to magnetic applications owing to their chemical stability and the reported uniaxial magnetocrystalline anisotropy of $K_u \sim 7 \times 10^6$ J m^{-3}.[17] A large anisotropy corresponds to a stable magnetic moment. The probability, P, of thermal activation reversing the magnetic axis of an individual nanoparticle scales as:

$$P \propto \exp\left(-\frac{K_u V}{k_B T}\right) \quad (1)$$

where V is the particle volume, k_B is Boltzman's constant, and T is temperature. Even room temperature is sufficient to induce fluctuations in the magnetic moments in small crystals of most materials. For this reason, highly anisotropic nanoscale FePt particles, which are unusually well protected from unwanted magnetization reversals, have become likely candidates for future ultrahigh-density recording media.[18] Synthesis of FePt nanoparticles is based on the polyol process as described by Sun et al.[19] As prepared, these nanocrystals are in a chemically disordered face-centered cubic (fcc) phase and require annealing above 803 K to achieve the high-K_u $L1_0$ face-centered tetragonal (fct) phase. This annealing process has proven problematic in that the nanoparticles tend to coalesce at high temperatures, thereby defeating the advantage of small, dispersed FePt particles for recording applications.[20] Recent work has shown, however, that the coalescence can be prevented by using suitable linker molecules or oxide coatings, and there are reports that the fct phase can even be directly synthesized.[21–24] For the present study, we have chosen to work with fcc FePt to establish the effectiveness of the polymeric-templating methodology. Since the assembly is driven by interactions between the surfactant capping molecules and the polymer substrate, the magnetization of the core is assumed to play a negligible role. Creating ordered nanostructures with the $L1_0$ phase remains the long-term goal.

The asymmetric poly(styrene)-*block*-poly(methyl methacrylate) (PS-*b*-PMMA) diblock copolymer used in this study has 29 wt.-% PMMA, so in the bulk it forms hexagonally packed PMMA cylinders in a PS matrix with a natural layer thickness (L) of 30 nm. Using the procedure outlined in the experimental section, we achieved films with an average thickness of L, which have an unusual dual presentation of PS and PMMA at the air interface due to the half-cylinder structure resulting from similar surface energies for the blocks.[25] These laterally alternating domains have significant short-range order but form "fingerprint" patterns with no long-range order unless guided by external constraints.[26,27] The FePt nanoparticle deposition procedure described in the Experimental section leads to nanocrystal cluster surface densities of approximately 100/μm^2. One can adjust the coverage by manipulating the solution concentration, but higher concentrations typically lead to excessive unwanted aggregation of the nanoparticles. Another route to obtain higher coverage is to perform multiple depositions using the procedure outlined above. Following three successive castings, we obtained cluster densities on the surface of ~300/μm^2.

Structural characterization of the FePt/PS-*b*-PMMA system can be achieved using scanning or transmission electron microscopy (SEM or TEM) or atomic force microscopy (AFM). High-energy electrons from SEM and TEM have a high propensity to damage both the polymer film and the organic surfactant molecules surrounding the FePt cores, so AFM was used in these experiments. Imaging with AFM requires careful tuning of the tapping conditions. The selection of the tapping mode AFM imaging parameters, in particular the tip driving amplitude, has a significant effect, not only on what one observes but also on the structure of the system itself. Very light tapping (~50 mV) allows one to image the nanoparticles resting on the polymer film, but not the fingerprint domains of the polymer. The PS-*b*-PMMA cylindrical structure becomes apparent along with the nanoparticles as the driving amplitude is increased to moderate levels (100–200 mV). This is the imaging regime used to analyze the selectivity of nanoparticle adsorption. When the amplitude is intensified by a further 200 % (~300 mV), many of the nanocrystals are pushed into the polymer matrix or dragged across the surface by the tip. While a precise determination of the minimum AFM tip force necessary to move the nanoparticles is made difficult by complex interactions between the tip and the soft substrate,[28] various theoretical analyses suggest the imaging conditions discussed above produce peak forces of the order of 40 nN.[29–32] These effects are readily observed by repeatedly imaging the same region under hard tapping conditions and watching individual nanoparticles disappearing or plowing troughs through the polymer as they are pulled along. Care was taken during this study to prevent tip influences on the nanoparticle positions.

Nanoparticle adsorption on the as-prepared films exhibited a moderate preference for the PS domains with 50–80 % of the FePt residing there (not shown), guided by the hydrophobic interactions between styrene and the alkane tails of the oleic acid capping molecules. The distribution of nanoparticles between the two domains displayed significant variation between different samples despite similar preparation conditions. In order to maximize the selectivity and strengthen the nanoparticle–substrate communication, one must modify the chemistry of the polymer and/or the capping molecules. Dual-surface presentation of these PS-*b*-PMMA films is a rare characteristic that is convenient for templating applications, so it is more straightforward to alter the chemistry post-casting rather than to begin with a different diblock copolymer material.

We modified the polymer templates with vacuum ultraviolet (VUV) radiation prior to FePt deposition. Fourier-transform infrared (FTIR) spectroscopy, ultraviolet photoelectron spectroscopy, mass spectrometry, and NMR studies with

ADVANCED MATERIALS

PMMA homopolymer reported in the literature have been used to characterize its response to high-energy irradiation, including VUV as used herein.[33–35] PMMA reacts through several routes: severing the C–C main-chain bonds, cleaving ester side-chain linkages, and generating C=C bonds in the backbone. PS is believed to crosslink under VUV exposure resulting in a chemical presentation at the interface similar to that present before irradiation. Therefore, our process is expected to selectively etch away the PMMA half-cylinders leaving a highly corrugated PS surface; this has been verified by means of AFM (Fig. 1). Figure 2 depicts FTIR spectra of the PS-*b*-PMMA film before and after VUV irradiation. Spectra of PS and PMMA homopolymers (not shown) reveal that the decay of the peak centered at ~1730 cm^{-1}, characteristic of a C=O stretch (see inset), is indicative of PMMA degradation. The chemical moieties displayed within the etched regions are inferred to be a combination of methyl methacrylate fragments and oxidized radical bonds. These more reactive species attract the nanoparticles to the etched domains. This results in two notable changes: 1) a reversal of the FePt domain selectivity when compared with the original film, i.e., from PS to etched PMMA; and 2) a significantly higher degree of selectivity (Fig. 3). A possible alternative explanation is that solvent de-wetting plays a role in the deposition within the troughs, because, as the FePt solution dries during spin-casting, the edge of the droplet may hesitate momentarily when it encounters each etched domain, thereby allowing more time for nanoparticles to deposit onto the surface in these regions.[36] We have tested this latter, kinetic hypothesis by heating the FePt/VUV-PS-*b*-PMMA system to 367 K, just below the PS-*b*-PMMA glass-transition temperature (T_g = 378 K), and have determined that the adsorption selectivity presented in Figure 3 is thermodynamically stable and hence likely driven by chemical interactions rather than de-wetting be-

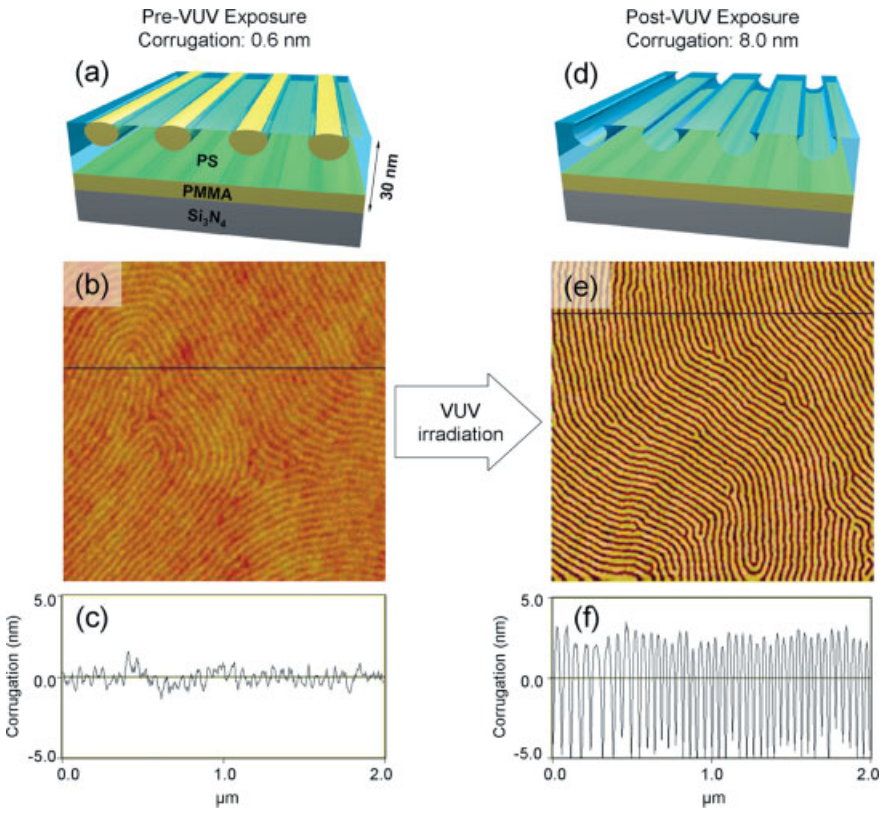

Figure 1. Effect of VUV irradiation on a PS-*b*-PMMA ultrathin film depicted in schematic form (a,d), with tapping mode AFM phase images (2 μm × 2 μm) (b,e), and with line scans showing surface corrugation (c,f). Pre-exposure surface corrugation is ~0.6 nm, with the PMMA phase appearing brighter (higher). VUV irradiation causes selective etching of the surface PMMA half-cylinders resulting in a corrugation of ~8 nm. The etched surface is a highly selective template for the adsorption of FePt colloidal nanoparticles.

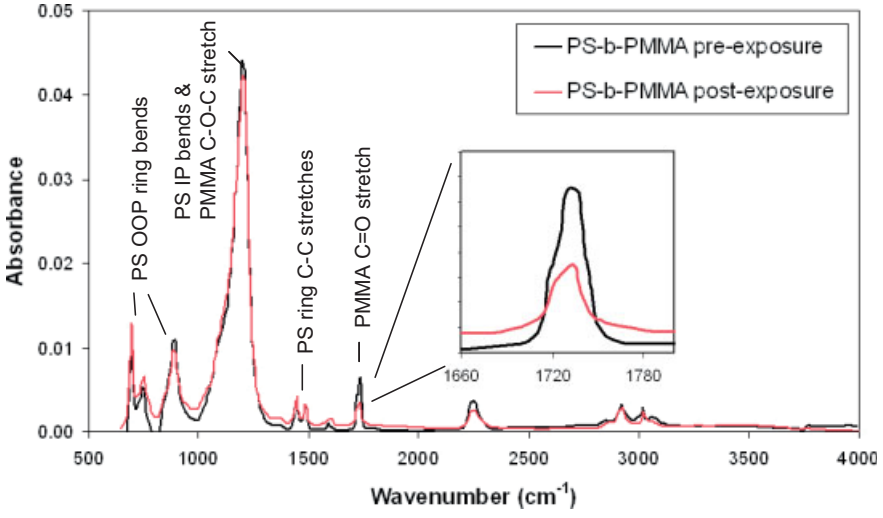

Figure 2. FTIR spectra of PS-*b*-PMMA before (black) and after (red) VUV irradiation. Decay of the C=O stretching vibration peak centered at ~1730 cm^{-1} indicates etching of the PMMA domains. It does not fully disappear because there is still an intact PMMA layer in contact with the silicon nitride substrate. IP and OOP stand for in-plane and out-of-plane, respectively.

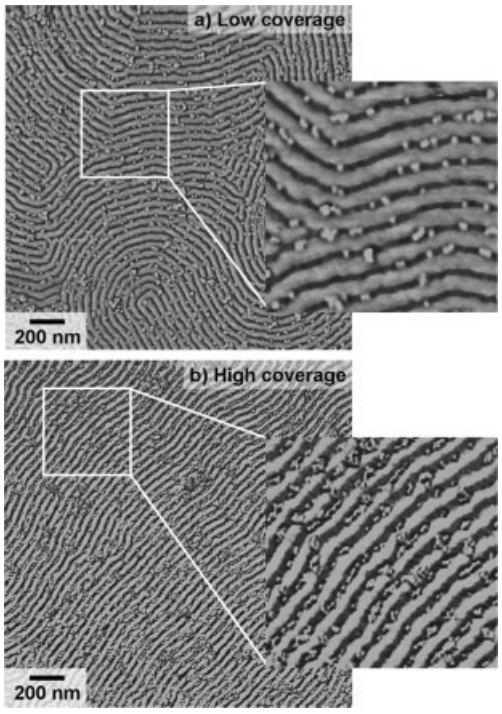

Figure 3. Representative 2 μm × 2 μm tapping mode AFM phase images showing ~99 % selective adsorption of single FePt nanoparticles onto the photochemically modified polymer domains (dark stripes) with a) low coverage (~100 clusters/μm^2) and b) high coverage (~225 clusters/μm^2). Increasing the coverage results in a somewhat larger population of multiparticle clusters but does not reduce the overall selectivity of the single particles.

havior. Indeed, further indication of the attractive interactions is that the nanoparticles do not even migrate *within* the etched domains during annealing.

While the as-synthesized nanoparticles exist primarily as isolated single particles in dilute solution mediated by the solvent, they have a tendency to aggregate into small clusters during deposition due to attractive van der Waals' interactions between the surfactant capping molecules. As the solvent evaporates during spin-casting the concentration of the deposited nanoparticle solution increases, thereby inhibiting the ability of the solvent to prevent aggregation. Clusters containing two particles represent 20 % of the surface population, and those containing three or more particles represent 30 %. The remaining 50 % are isolated nanoparticles. A statistical analysis of numerous AFM images reveals that 99 % of the single FePt nanoparticles adhere to the exposed PMMA phase. Larger clusters often adsorb partially onto the PS phase because their dimensions are comparable to, or larger than, the polymer microdomain spacing. Those larger clusters that have a linear aspect ratio, i.e., nanoparticle chains, also exhibit a high selectivity for the etched regions and align such that their long axis is parallel to the channels. Taken together, these data demonstrate that exposing a PS-*b*-PMMA film to VUV radiation results in a superior template for nanoparticle adsorption. Remaining challenges include minimizing nanoparticle aggregation while increasing the overall surface coverage and obtaining the high anisotropy fct-FePt phase without inducing interparticle sintering. A related issue important for future applications and fundamental investigations of one- and two-dimensional nanoparticle interactions is the spatial ordering of the nanocrystals within the channels. We are investigating the driving forces that govern this ordering with the aim of ultimately gaining control of both the interparticle spacing and the long-range order.

In summary, we report a novel approach for obtaining self-organized assemblies of magnetic nanoparticles using a modified polymeric template. A PS-*b*-PMMA diblock copolymer thin film was irradiated with VUV light to selectively etch the surface PMMA domains thereby producing a corrugated organic substrate. The exposed film was used as a template for the self-assembly of oleic acid-capped FePt nanocrystals that adsorb with nearly 100 % selectivity within the photochemically created nanoscopic channels. Ramifications of this work extend to potential future bit-patterned magnetic-storage media. The method does not rely on the magnetic character of the FePt core. It is, therefore, general to all surfactant-mediated nanoparticles suggesting possible applications in the templating of electronic, photonic, and catalytic systems.

Experimental

Asymmetric PS-*b*-PMMA with a molecular weight of 77 000 g mol^{-1} and a polydispersity of 1.09 was obtained from Polymer Source. Excess PS homopolymer was removed via Soxhlet extraction in cyclohexane. Thin films were then spin-cast at 5000 rpm from 1.5 wt.-% toluene solution onto clean silicon nitride substrates and annealed for six hours at 518 K in an inert atmosphere. FePt nanoparticles were deposited onto prepared polymer films via spin-coating a 5 μl drop of dilute octane solution (~0.5 wt.-%) at 3000 rpm. Imaging was performed on a Digital Instruments Nanoscope IV using Veeco tapping-mode etched silicon tips (radius of curvature ~ 10 nm, spring constant ~ 40 N m^{-1}). VUV irradiation was carried out at pressures of ~2×10^{-7} torr (1 torr = 133.32 Pa) using a Hamamatsu L2793 deuterium lamp with a MgF_2 window. This configuration provides continuum spectral output in the range 115–400 nm, with an average intensity of 8×10^{-6} J cm^{-2} s^{-1}. Typical exposures times were 7–15 min.

Received: May 11, 2005
Final version: June 17, 2005
Published online: August 22, 2005

[1] C. Park, J. Yoon, E L. Thomas, *Polymer* **2003**, *44*, 6725.
[2] F. S. Bates, G. H. Fredrickson, *Physics Today* **1999**, *52*, 32.
[3] M. Park, C. Harrison, P. M. Chaikin, R. A. Register, D. H. Adamson, *Science* **1997**, *276*, 1401.
[4] R. A. Segalman, H. Yokoyama, E. J. Kramer, *Adv. Mater.* **2001**, *13*, 1152.
[5] J. Y. Cheng, C. A. Ross, E. L. Thomas, H. I. Smith, G. J. Vancso, *Adv. Mater.* **2003**, *15*, 1599.
[6] S. B. Darling, S. D. Bader, *J. Mater. Chem.* 2005, DOI: 10.1039/b506357d.
[7] D. Sundrani, S. B. Darling, S. J. Sibener, *Nano Lett.* **2004**, *4*, 273.
[8] D. Sundrani, S. B. Darling, S. J. Sibener, *Langmuir* **2004**, *20*, 5091.
[9] S. O. Kim, H. H. Solak, M. P. Stoykovich, N. J. Ferrier, J. J. D. Pablo, P. F. Nealey, *Nature* **2003**, *424*, 411.

ADVANCED MATERIALS

[10] R. W. Zehner, W. A. Lopes, T. L. Morkved, H. Jaeger, L. R. Sita, *Langmuir* **1998**, *14*, 241.
[11] R. W. Zehner, L. R. Sita, *Langmuir* **1999**, *15*, 6139.
[12] M. R. Bockstaller, Y. Lapetnikov, S. Margel, E. L. Thomas, *J. Am. Chem. Soc.* **2003**, *125*, 5276.
[13] Y. Lin, A. Böker, J. He, K. Sill, H. Xiang, C. Abetz, X. Li, J. Wang, T. Emrick, S. Long, Q. Wang, A. Balazs, T. P. Russell, *Nature* **2005**, *434*, 55.
[14] J. Y. Cheng, C. A. Ross, V. Z. Chan, E. L. Thomas, R. G. H. Lammertink, G. J. Vancso, *Adv. Mater.* **2001**, *13*, 1174.
[15] M. Bal, A. Ursache, M. T. Tuominen, J. T. Goldbach, T. P. Russell, *Appl. Phys. Lett.* **2002**, *81*, 3479.
[16] L. Cao, J. A. Massey, M. A. Winnik, I. Manners, S. Riethmüller, R. Banhart, J. P. Spatz, M. Möller, *Adv. Funct. Mater.* **2003**, *13*, 271.
[17] O. A. Ivanov, L. V. Solina, V. A. Demshina, L. M. Magat, *Phys. Met. Metallogr.* **1973**, *35*, 81.
[18] X. Yang, C. Liu, J. Ahner, J. Yu, T. Klemmer, E. Johns, D. Weller, *J. Vac. Sci. Technol., B* **2004**, *22*, 31.
[19] S. Sun, C. B. Murray, D. Weller, L. Folks, A. Moser, *Science* **2000**, *287*, 1989.
[20] Z. R. Dai, S. Sun, Z. L. Wang, *Nano Lett.* **2001**, *1*, 443.
[21] M. Mizuno, Y. Sasaki, A. C. C. Yu, M. Inoue, *Langmuir* **2004**, *20*, 11 305.
[22] C. Liu, X. Wu, T. Klemmer, N. Shukla, D. Weller, A. Roy, M. Tanase, D. Laughlin, *Chem. Mater.* **2005**, *17*, 620.
[23] B. Jeyadevan, K. Urakawa, A. Hobo, N. Chinnasamy, K. Shinoda, K. Tohji, D. D. J. Djayaprawira, M. Tsunoda, M. Takahashi, *Jpn. J. Appl. Phys., Part 2* **2003**, *42*, L350.
[24] X. Teng, H. Yang, *J. Am. Chem. Soc.* **2003**, *125*, 145 59.
[25] T. L. Morkved, H. M. Jaeger, *Europhys. Lett.* **1997**, *40*, 643.
[26] J. Hahm, W. A. Lopes, H. M. Jaeger, S. J. Sibener, *J. Chem. Phys.* **1998**, *109*, 10 111.
[27] E. Huang, P. Mansky, T. P. Russell, C. Harrison, P. M. Chaikin, R. A. Register, C. J. Hawker, J. Mays, *Macromolecules* **2000**, *33*, 80.
[28] F. Dubourg, J. P. Aimé, *Surf. Sci.* **2000**, *466*, 137.
[29] J. Tamayo, R. García, *Langmuir* **1996**, *12*, 4430.
[30] R. García, A. S. Paulo, *Phys. Rev. B* **1999**, *60*, 4961.
[31] A. S. Paulo, R. García, *Phys. Rev. B* **2002**, *66*, 041 406.
[32] R. W. Stark, W. M. Heckl, *Surf. Sci.* **2000**, *457*, 219.
[33] P. W. Bohn, J. W. Taylor, H. Guckel, *Anal. Chem.* **1981**, *53*, 1082.
[34] K. K. Okudaira, S. Hasegawa, P. T. Sprunger, E. Morikawa, V. Saile, K. Seki, Y. Harada, N. Ueno, *J. Appl. Phys.* **1998**, *83*, 4292.
[35] A. Gupta, R. Liang, F. D. Tsay, J. Moacanin, *Macromolecules* **1980**, *13*, 1696.
[36] R. D. Deegan, O. Bakajin, T. F. Dupont, G. Huber, S. R. Nagel, T. A. Witten, *Nature* **1997**, *389*, 827.

A Reagentless Biosensing Assembly Based on Quantum Dot–Donor Förster Resonance Energy Transfer**

By *Igor L. Medintz*,* *Aaron R. Clapp*, *Joseph S. Melinger*, *Jeffrey R. Deschamps*, and *Hedi Mattoussi**

Reagentless biosensors combine the specific recognition of biochemical receptors, usually proteins, with the ability to concomitantly produce quantitative output data that does not require further processing. These biosensors can help meet the growing analytical demands in diverse applications such as healthcare, security, food and water assurance, environment, and industrial process monitoring.[1,2] Bacterial periplasmic binding proteins (bPBPs) have provided many of the biorecognition elements used in reagentless biosensors, targeting various sugar, peptide, and ion analytes.[3,4] Upon binding of a specifically recognized analyte in their binding pockets, these hinge-bending proteins undergo an obligatory conformational change. Cass and co-workers have demonstrated that judicious placement of a dye within the maltose-binding protein (MBP) structure allows fluorescent signaling of changes in maltose concentration, derived from changes in the dye emission.[5] MBP has further served as a versatile platform for testing various reagentless biosensing modalities including redox-active sensing and an elegant fluorescence resonance-energy transfer (FRET)-based multifluorescent protein–MBP fusion sensor.[6,7] Hellinga and co-workers have also shown that the binding pocket of bPBPs could be remodeled to target non-natural analytes, such as trinitrotoluene (TNT), using computationally intensive redesign and muta-

[*] Dr. I. L. Medintz
Center for Bio/Molecular Science and Engineering
Code 6900, U.S. Naval Research Laboratory
Washington, DC 20375-5320 (USA)
E-mail: Imedintz@cbmse.nrl.navy.mil
Dr. H. Mattoussi, Dr. A. R. Clapp
Division of Optical Sciences
Code 5611, U.S. Naval Research Laboratory
Washington, DC 20375-5320 (USA)
E-mail: Hedimat@ccs.nrl.navy.mil
Dr. J. S. Melinger
Electronics Science and Technology Division
Code 6800, U.S. Naval Research Laboratory
Washington, DC 20375-5320 (USA)
Dr. J. R. Deschamps
Laboratory for the Structure of Matter
Code 6812, U.S. Naval Research Laboratory
Washington, DC 20375-5320 (USA)

[**] The authors acknowledge NRL and A. Ervin and L. Chrisey at the Office of Naval Research (ONR grant no. N001404WX20270) and A. Krishnan at DARPA for support. A. R. C. is supported by a National Research Council Fellowship through NRL. Supporting Information is available online from Wiley InterScience or from the author.

  DOI: 10.1002/adma.200500722